



CHALMERS
UNIVERSITY OF TECHNOLOGY

Transfer-free, lithography-free and fast growth of patterned CVD graphene directly on insulators by using sacrificial metal catalyst

Downloaded from: <https://research.chalmers.se>, 2021-08-31 19:55 UTC

Citation for the original published paper (version of record):

Dong, Y., Xie, Y., Xu, C. et al (2018)



Transfer-free, lithography-free and fast growth of patterned CVD graphene directly on insulators by using sacrificial metal catalyst

Nanotechnology, 29(36)

<http://dx.doi.org/10.1088/1361-6528/aacce>

N.B. When citing this work, cite the original published paper.

Transfer-free, lithography-free and fast growth of patterned CVD graphene directly on insulators by using sacrificial metal catalyst

Yibo Dong¹, Yiyang Xie¹, Chen Xu^{1,3}, Yafei Fu¹, Xing Fan¹, Xuejian Li¹,
Le Wang¹, Fangzhu Xiong¹, Weiling Guo¹, Guanzhong Pan¹ ,
Qihua Wang¹, Fengsong Qian¹ and Jie Sun^{1,2,3} 

¹Key Laboratory of Optoelectronics Technology, College of Microelectronics, Beijing University of Technology, Beijing 100124, People's Republic of China

²Quantum Device Physics Laboratory, Department of Microtechnology and Nanoscience, Chalmers University of Technology, Gothenburg SE-41296, Sweden

E-mail: xuchen58@bjut.edu.cn and jie.sun@chalmers.se

Received 16 May 2018, revised 10 June 2018

Accepted for publication 14 June 2018

Published 28 June 2018



CrossMark

Abstract


Chemical vapor deposited graphene suffers from two problems: transfer from metal catalysts to insulators, and photoresist induced degradation during patterning. Both result in macroscopic and microscopic damages such as holes, tears, doping, and contamination, translated into property and yield dropping. We attempt to solve the problems simultaneously. A nickel thin film is evaporated on SiO₂ as a sacrificial catalyst, on which surface graphene is grown. A polymer (PMMA) support is spin-coated on the graphene. During the Ni wet etching process, the etchant can permeate the polymer, making the etching efficient. The PMMA/graphene layer is fixed on the substrate by controlling the surface morphology of Ni film during the graphene growth. After etching, the graphene naturally adheres to the insulating substrate. By using this method, transfer-free, lithography-free and fast growth of graphene realized. The whole experiment has good repeatability and controllability. Compared with graphene transfer between substrates, here, no mechanical manipulation is required, leading to minimal damage. Due to the presence of Ni, the graphene quality is intrinsically better than catalyst-free growth. The Ni thickness and growth temperature are controlled to limit the number of layers of graphene. The technology can be extended to grow other two-dimensional materials with other catalysts.

Supplementary material for this article is available [online](#)

Keywords: transfer-free, lithography-free, graphene, chemical vapor deposition, insulating substrate

(Some figures may appear in colour only in the online journal)

³ Authors to whom any correspondence should be addressed.

 Original content from this work may be used under the terms of the [Creative Commons Attribution 3.0 licence](#). Any further distribution of this work must maintain attribution to the author(s) and the title of the work, journal citation and DOI.

1. Introduction

As a truly two-dimensional (2D) material, graphene has received worldwide attention due to its unique combination of many special properties such as high carrier mobility, high transmittance and gapless energy band [1, 2]. It may play an important role in future electronics, energy and biomedicine

spheres. The synthesis of graphene is the upstream sector in future graphene based industries, occupying a critical position in the advancement of graphene research towards commercialization. Today, the graphene synthesis includes several techniques, such as micromechanical exfoliation [3], reduction of graphene oxide [4–6], epitaxial growth [7, 8] and chemical vapor deposition (CVD) [9–11]. Among them, CVD is very promising in terms of its scalability, high material quality and relatively low cost. Usually, the CVD method requires growing graphene on catalytic metals (Cu, Ni, etc). However, as the substrates are conducting, which will cause a short circuit, it is not possible to fabricate electronic devices therein. The graphene has to be transferred to foreign insulating or semiconducting substrates. The transfer of one atomic layer carbon, however, is complicated and of low efficiency. Even more seriously, it inevitably leaves extra defects e.g. wrinkles, holes, and contaminants in the graphene, constituting the biggest obstacle in the way to industrialization. For this reason, many CVD approaches have been developed to synthesize graphene samples on insulating substrates.

Currently, the direct growth strategies of graphene can be roughly categorized into three kinds [12]: metal-free growth [13, 14], plasma enhanced CVD [15, 16], and sacrificial metal assisted growth [17–20]. The metal-free deposition has almost no requirement on the substrates (need to be high temperature stable though), and the graphene is uniform, but it generally needs a long growth time and/or very high temperature (sometimes $>1000\text{ }^{\circ}\text{C}$), and the material quality is typically low. The plasma method can effectively reduce the deposition temperature ($<800\text{ }^{\circ}\text{C}$). Nevertheless, the controllability over the number of layers is poor, and the material quality is not high either. The third method uses metals to assist the growth. A thin metal layer (Cu or Ni) is deposited on substrate, and graphene is grown at the metal-substrate interface [17, 19, 20]. Because of the existence of a catalyst, the graphene quality is boosted, and the growth temperature is limited to no more than $1000\text{ }^{\circ}\text{C}$. However, during the process of reproducing these results [17, 19], we discovered that the repeatability of this method is not high and upon etching of the metals, the graphene beneath the metals tends to crack (see figure S1, available online at stacks.iop.org/NANO/29/365301/mmedia). This may be due to carbon atoms needing to pass through the metal layer and the lack of polymer support during the metal etching process.

In this paper, we propose a new and facile method to grow graphene directly on insulating substrates by etching sacrificial metal catalyst through a PMMA support layer. As shown in figure 1(a), we grow graphene on the surface of Ni sacrificial layer instead of at the metal-substrate interface. As a result, this growth process is highly repeatable and controllable. Then, PMMA polymer is coated onto the sample as the mechanical support for graphene. PMMA is a common supporting layer material in the graphene transfer process because of its high mechanical strength. However, researchers rarely pay attention to its other characteristic, that etchant can permeate PMMA [11].

Using this characteristic, the Ni layer can be etched with a PMMA/graphene layer on its surface (figure S2). During the graphene growth, we control the morphology of Ni to enable PMMA to be fixed on the substrate, just like using nails to fix the four corners of the tent on the ground. After Ni is etched away, the graphene ‘lands’ on the substrate.

Using this technology, we manage to obtain large area continuous graphene with minimal damages. Furthermore, since this is catalytic growth, the area of graphene is determined by the area of Ni, which can be lithographically patterned. Hence, the graphene can be indirectly patterned, without getting in contact with photoresists. We note that graphene’s unintentional doping and contamination from the photoresists is a very big problem in the community [21]. Clearly, this problem is absent in our case. Using our technique, we have grown graphene on different substrates including Si with surface oxide (SiO_2/Si), quartz, and sapphire, and achieved μm -precision graphene patterns without performing a direct lithography in the graphene (lithography-free patterning). The whole deposition procedure, including the heating and cooling, is merely ~ 30 min, which is to our knowledge the shortest among the reported direct growth processes. The graphene is fully supported by the PMMA layer, resulting in almost zero mechanical damage. The as-developed method can be extended to other common graphene catalysts such as Cu (not limited to Ni).

2. Results and discussion

2.1. Process description and analysis

The graphene formation process is schematically demonstrated in figure 1(a) (for details, see the Experimental section). After the CVD process, a graphene film is grown on top of the Ni surface. Meanwhile, the Ni film on SiO_2/Si aggregates due to the high temperature, resulting in numerous holes with a few microns in diameter, as shown in figure 1(b). The Ni aggregation on quartz and sapphire substrates is shown in figure S3. The Ni aggregation normally does not occur until the temperature is close to $1000\text{ }^{\circ}\text{C}$. We introduce CH_4 into the chamber immediately after the $800\text{ }^{\circ}\text{C}$ annealing. It guarantees that there is graphene grown also in the holes, as the graphene is grown earlier than the Ni aggregation. The graphene will ‘land’ on the substrate when the Ni aggregation happens (similar effect has been observed on Cu [18]), and therefore the graphene forms a very continuous film on the substrate with minimal holes and tears. We note that the Ni aggregation has a positive effect in our experiments. As indicated by the red circle in figure 1(a), the PMMA/graphene film is anchored to the substrate via the μm -sized holes in the nickel film, which keeps the PMMA/graphene stable throughout the metal etching (otherwise the PMMA/graphene can be free standing when the metal is absent). This is useful for keeping the graphene morphology intact. During the 10 min Ni etching process, the etchant accesses the Ni both from sideways and by the front face diffusion through

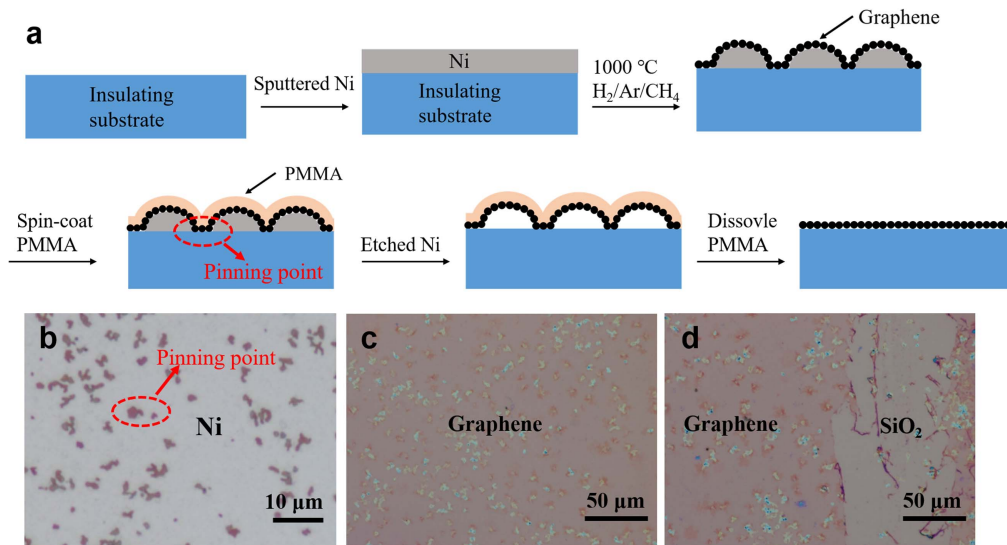


Figure 1. (a) Schematic illustration of our process of growing transfer-free graphene directly on insulating substrate via etching the sacrificial metal catalyst. The Ni can also be pre-patterned by photolithography to avoid the direct contact of graphene with photoresist. (b) Morphology of Ni after the graphene growth. (c) and (d) are optical images of the as-grown graphene after etching off the Ni catalyst.

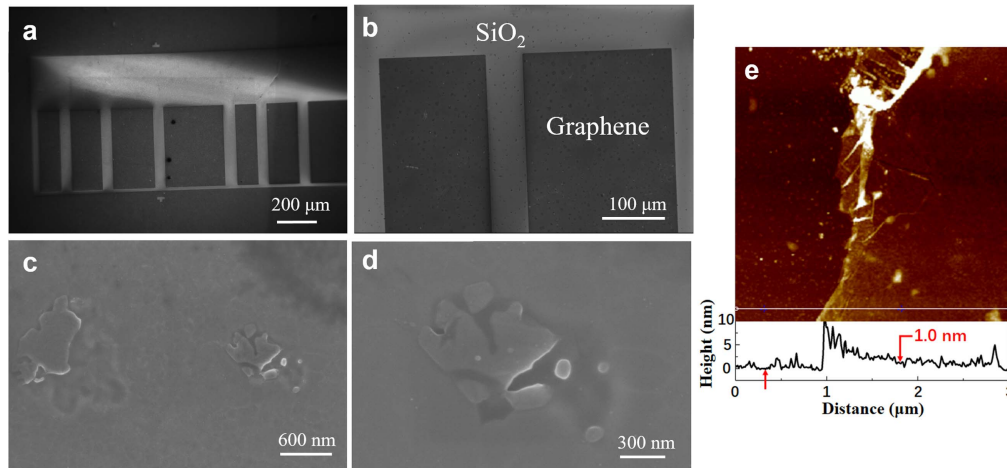


Figure 2. (a)–(d) SEM images of the as-grown graphene under different magnifications. (e) AFM image of the as-grown graphene over $3 \mu\text{m} \times 3 \mu\text{m}$ area. The height profile is measured along the white line in (e). The height difference between the two points indicated by the arrows is 1 nm.

the PMMA/graphene. It is known that the PMMA/graphene stack is permeable to liquid chemicals [11].

2.2. Material characterization

The x-ray photoelectron spectroscopy measurement of the as-prepared graphene is shown in figure S4, confirming its composition and chemical bond information. Figures 1(c) and (d) shows the micrographs of the transfer-free graphene, where the graphene is seen to be continuous in large area with almost no mechanical damages. We could not find any observable tears with an optical microscope, even at a magnification of $1000\times$ (there is an intentionally made tweezer scratch in figure 1(d) in order to see the contrast of the SiO_2 substrate.). Based on the uniformity in the color (300 nm SiO_2 on Si provides the possibility for approximate identification of

the number of layers by optical observation [22]), one can tell the graphene is largely uniform in terms of layers. However, we do discover many white marks in figures 1(c) and (d). The white marks can not be found at areas where Ni has not aggregated. That is to say, these marks occur at positions where holes form as a result of the Ni aggregation. These are also the places where Ni diffuses into SiO_2 , which will be discussed later.

Figures 2(a)–(d) show the scanning electron microscopy (SEM) images of the graphene, where the graphene in figures 2(a) and (b) is patterned in order to generate some contrast in the SEM. The graphene is homogeneous in the range of hundreds of microns. In figures 2(c) and (d), the white marks are seen again. Although the morphology is somewhat roughened at these points as a consequence of the Ni diffusion into SiO_2 , the graphene is still there (otherwise,

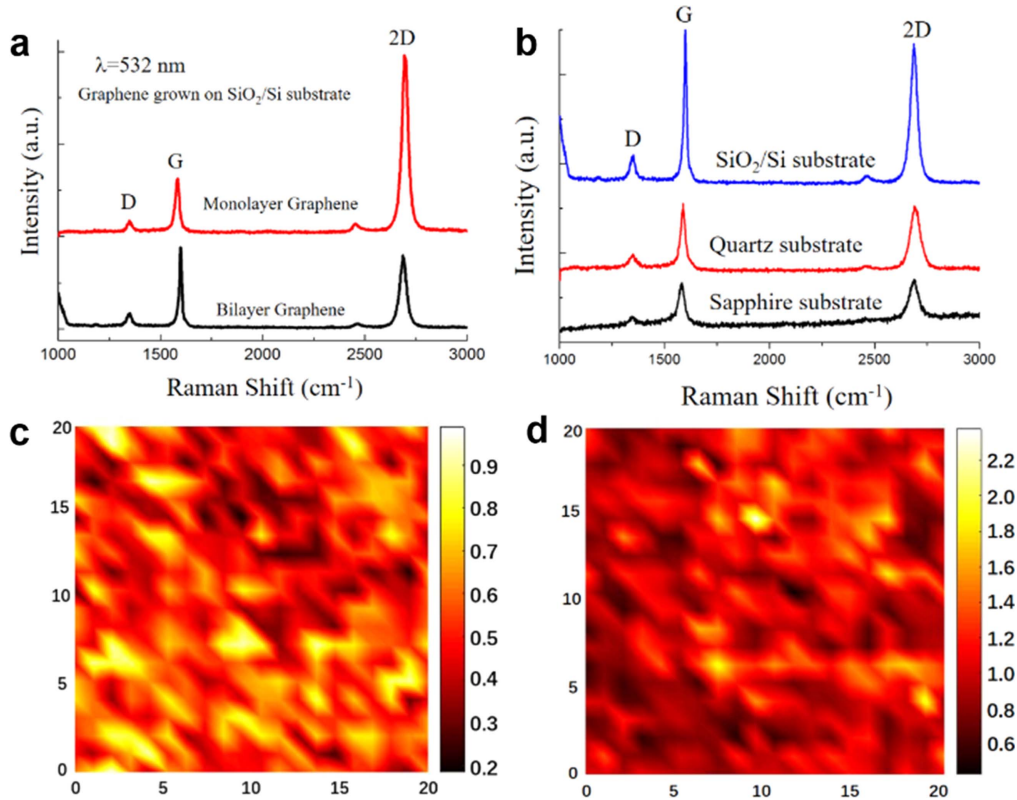


Figure 3. (a) Typical Raman spectra of the graphene grown on SiO₂/Si substrate. (b) Typical Raman spectra of the graphene grown on three different substrates. (c) and (d) are Raman mapping of the D/G and G/2D ratios of the graphene over 50 $\mu\text{m} \times 50 \mu\text{m}$ area, respectively. The graphene is relatively uniform.

the absence of graphene is very easy to identify, since it has a high contrast as shown in figures 2(a) and (b)). Hence, our graphene is continuous with minimal number of holes, which is certainly due to the fact that the most graphene is already grown before the Ni aggregation takes place. Figure 2(e) is an atomic force microscopy (AFM) image of the graphene. By scanning across the edge, the height of graphene is approximately 1.0 nm.

Figure 3(a) is the Raman signals measured from the graphene. Because of the segregation based growth mechanism of graphene on Ni [23], apart from monolayer graphene, bilayer graphene is also detected in the Raman spectroscopy [24]. In figure 3(a), typical parameters for monolayer (bilayer) graphene are: G peak at $\sim 1585 \text{ cm}^{-1}$ (1590 cm^{-1}), 2D peak at 2693 cm^{-1} (2690 cm^{-1}) with full width at half maximum of 35 cm^{-1} (40 cm^{-1}), D peak at 1348 cm^{-1} (1350 cm^{-1}), and G/2D ratio of $I_G/I_{2D} = 0.30$ (1.04). The small height of D peaks indicates the high quality of the directly grown graphene. Figure 3(b) shows the Raman spectra of graphene grown on three types of substrates, where they appear similar to each other. Figures 3(c) and (d) are the Raman mapping data measured in a $50 \mu\text{m} \times 50 \mu\text{m}$ area (20×20 points with $2.5 \mu\text{m}$ pitch). Figure 3(c) is the mapping of Raman D/G peak ratio, where I_D/I_G lies in the range of 0.18–0.99. Figure 3(d) shows the mapping of Raman G/2D peak ratio with I_G/I_{2D} of typically 0.43–2.38.

2.3. Cause of white marks

In our experiment, we find that the white marks appear at the places where Ni film aggregates to form tiny holes. We can see from SEM images in figures 2(c), (d) that these marks are not particles. The origin of these marks lies in the diffusion of Ni into the underlying SiO₂. The diffusion of Ni into SiO₂ causes the color change of SiO₂. We have prepared silicon substrates with 100 and 300 nm thick SiO₂ films, and found that the white marks on the 100 nm SiO₂ sample are more pronounced. Etching away the SiO₂, the Si substrate of the 100 nm sample exhibits a morphology change, shows many black dots, and also has a change in the substrate color, as shown in figure S5(a). In contrast, the Si substrate of the 300 nm SiO₂ sample basically remains unchanged (figure S5(b)). The Ni diffuses through the 100 nm SiO₂ and reacts with Si to form nickel silicide and causes the change in the substrate, whereas this effect is less pronounced in the 300 nm SiO₂ sample due to the thicker oxide. Interestingly, the diffusion of Ni is only observed at the aggregation induced holes. In the no aggregation areas, and in samples with thicker Ni film where aggregation is entirely absent, we have not found any white marks. At the same time, we find that the graphene grown in these white mark regions is of higher quality as proved by the lower D peak (see figures 4(a) and (b)). This is a general effect rather than an isolated case, as seen in the Raman mapping in figure S6. The phenomenon is understandable. The metal in the aggregating

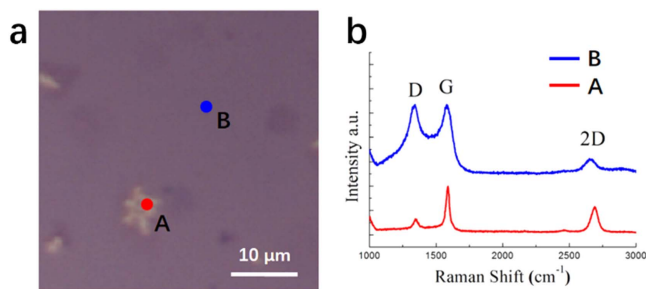


Figure 4. (b) Raman spectra taken at positions A and B indicated in the optical image in (a).

areas is in liquid form locally. It has a smooth surface without any grain boundaries, together with a higher migration speed of the carbon atomic species. It naturally leads to fewer defects in the graphene [25–27]. Due to its higher local temperature, liquid metal also has a stronger ability of diffusion and permeation in the SiO_2 . In fact, the underlying reason for the Ni aggregation is because the liquid metal does not wet some substrates such as SiO_2 and sapphire due to their lower surface energies. Similarly, the liquid Cu used in [25–27] wets tungsten, but not SiO_2 .

2.4. Effects of PMMA and morphology of Ni in metal etching

PMMA is a polymer with very high mechanical strength (Young's modulus of ~ 3.3 GPa [28]) and can dramatically reduce the damage in graphene during the metal etching, since otherwise the graphene will be free-standing when the Ni is removed. However, the PMMA film can not be regarded as an effective barrier for the etchant. It is known that liquid can penetrate very thin PMMA [11]. Although perfect graphene is not permeable to microscopic particles except protons [29], practical CVD graphene inevitably has some lattice defects and tears (figure S7), and thus can be penetrated by these particles. Therefore, one can not have the simple scenario that the etching is performed only through sideways. In fact, the direct etching via the front surface of Ni can not be ignored, which greatly boosts the etching speed.

The morphology of Ni also has a large influence on the final graphene integrity and quality. In our experiments, the optimal Ni morphology is that it aggregates into a somewhat holey, but yet continuously connected structure. The holey film has two advantages. First, as mentioned before, the tiny holes help fix the PMMA/graphene onto the substrate. Second, graphene grown at the hole areas and their vicinity has superior quality. Nevertheless, the holes must be controlled within a certain limit, because otherwise the Ni film will turn into many isolated islands (e.g. at elevated growth temperatures). It will not only reduce the integrity of the grown graphene, but also decrease the etching speed, since the etching solution can not transport freely between islands, as demonstrated in figure S8.

2.5. Thickness of Ni film

There are mainly two reasons why we choose to use 50 nm thick nickel. First, it can control the number of layers in the graphene. When monolayer graphene is grown on a catalytic metal film, its surface is covered and the direct contact of the

catalyst with the carbon precursor is suppressed, which is known as the self-limiting growth mechanism [10]. However, on metals with high carbon solubility such as Ni, the formation of bilayer and multilayer graphene is very common due to the additional graphene growth from the carbon reservoir in the bulk catalyst. Nevertheless, this segregation effect is very limited in our case. At 1000°C , 50 nm Ni dissolves $5.75 \times 10^{15} \text{ cm}^{-2}$ carbon atoms [30], whereas monolayer graphene contains $3.8 \times 10^{15} \text{ cm}^{-2}$ carbon atoms [20]. That is to say, the carbon dissolved in the 50 nm Ni is not yet enough for two layers of graphene, even if we assume it could be totally used on forming graphene. Therefore, the 50 nm Ni guarantees that the as-deposited graphene is ultrathin, drastically different from the case on bulk Ni catalyst. Meanwhile, it is necessary to note that although we can not exclude the possibility that there might be a small amount of graphene fragments between the nickel and the substrate, we have not observed noticeable graphene deposition beneath the Ni film through carbon segregation effect. Second, at 1000°C , 50 nm Ni easily turns into the optimal morphology shown in figure 1(b). On the other hand, if thicker nickel films are chosen (such as 100 nm), the aggregation effect is absent under our condition at 1000°C .

2.6. Lithography- and contamination-free patterning of graphene

By lithography-free we mean the lithography is only carried in our catalyst, but not the graphene. After photolithography, sputtering, lift-off, patterned Ni films are fabricated. As the growth is catalytic, the shape of graphene should follow that of the catalyst. The separation of graphene from its direct lithography not only simplifies the process, but also avoids the p-type doping and other contaminations resulted from the contact of graphene to the photoresists [21]. In fact, today the deterioration effect from the photoresist is one of the major causes of graphene's electrical property degradation. Our method elegantly bypasses this obstacle and can be applied to any common graphene catalysts such as Ni and Cu (the patterned growth on Cu can be found in figure S9.). In figure 5(a), Ni grids are lithographically manufactured. The SiO_2 can be seen in the $20 \mu\text{m} \times 20 \mu\text{m}$ windows. Because of the existence of these windows, the Ni aggregation is not necessary in terms of facilitating the anchoring of the PMMA film to the SiO_2 . Thus, we have attempted to use a Ni catalyst layer as thick as 250 nm (other growth conditions remain unchanged). Figure 5(b) shows the optical image of the graphene after etching off the sacrificial metal, where the darker dots are graphene of thicker layers. The graphene and Ni patterns look essentially the same. Clearly, without the Ni aggregation effect, no white marks have been observed, in consistence with the previous argument. Figure 5(c) is the Raman 2D peak mapping of the same graphene sample. Not surprisingly, the pattern reproduces the shape in figures 5(a) and (b). Compared with the 50 nm unpatterned Ni, the graphene grown on thicker and patterned Ni is more controllable and robust in the process, and the SiO_2 will not be damaged

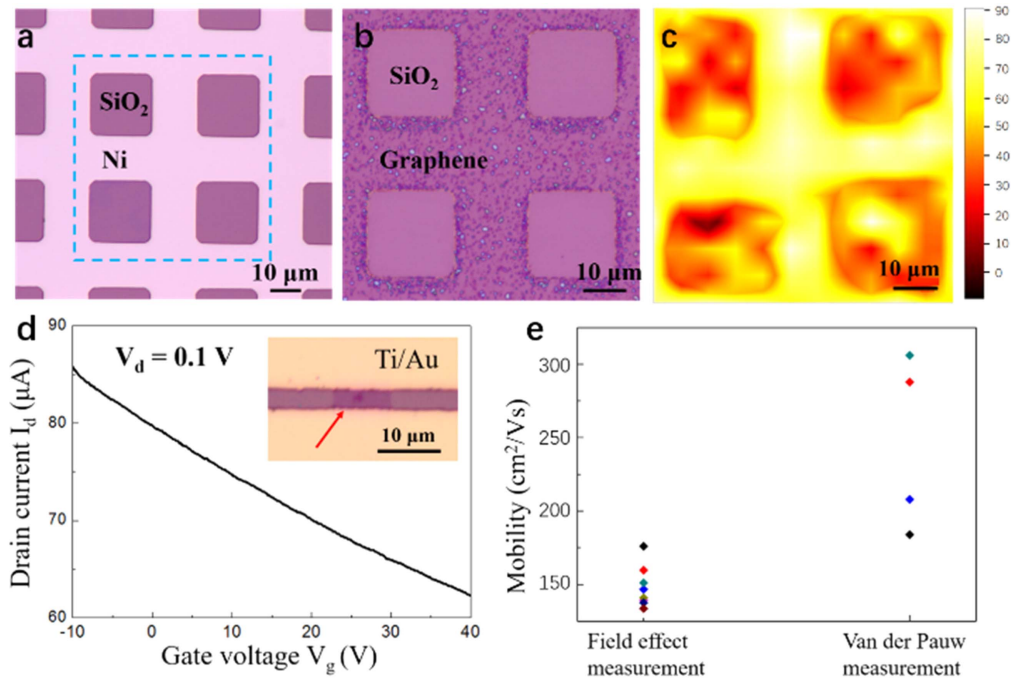


Figure 5. (a) and (b) are optical images of the patterned sample after the depositions of (a) Ni and (b) graphene. In (b), the metal is already etched away. (c) is the Raman mapping of the 2D peak of the graphene pattern. (d) Transfer curve (drain current I_d versus gate voltage V_g) for a GFET prepared from the as-grown graphene. The inset shows the photograph of the device. (e) Statistical field-effect mobility data for the devices made from field-effect measurement and van der Pauw measurement.

by the Ni, but at the expense of having more multilayer graphene patches.

2.7. Electrical measurements

We have fabricated back gated graphene field-effect transistors (GFETs) via 50 nm sacrificial Ni thin film. The dimension of the transistor channel is $L:W = 3 \mu\text{m}:9 \mu\text{m}$, where L and W are the channel length and width, respectively. Figure 5(d) demonstrates the transfer characteristics of an as-fabricated graphene FET, where the inset is the corresponding optical image. The field-effect mobility can be calculated by linear fitting of the slope $\Delta I_d / \Delta V_g$, which can be written as $\mu = (L/W C_{\text{ox}} V_d) (\Delta I_d / \Delta V_g)$ (C_{ox} is the gate capacitance) [17]. Through measuring eight graphene FETs, the carrier mobility is up to $175.98 \text{ cm}^2 \text{ V}^{-1} \text{ s}^{-1}$, as shown in figure 5(e) together with the data dispersion. The mobility is also measured through Hall effect via the van der Pauw method. In total for the four devices, the peak value for the Hall mobility is $306 \text{ cm}^2 \text{ V}^{-1} \text{ s}^{-1}$ with the sheet resistance being $1990 \Omega/\square$. The dispersion is shown in figure 5(e). Apparently, the field-effect mobility has been underestimated, possibly due to the not rigorous model and parameters. Anyway, the carrier mobility is lower than expected. The major reason is that the graphene has been patterned by ordinary photolithography and the resist has led to the mobility degrading and severe p-type doping, which is seen in figure 5(d). The practical reason that we have not implemented our lithography-free patterning of the graphene here is because even if we can avoid the lithography at this step, the graphene will anyhow be contaminated by photoresist during the second step lithography in the metal pads. One solution is to pattern the metal contacts beforehand and then deposit the graphene. In that

case the metal can not be gold based and needs to be high temperature compatible, e.g. Pt, Ti, etc. It is subject to future studies and the mobility is expected to increase significantly. A minor reason causing the mobility drop is, as discussed before, that some parts of the graphene are already directly deposited on the SiO_2 when the 50 nm Ni aggregates. The graphene has very tight contact with the SiO_2 due to the high temperature process [13, 17, 31], where the charged impurities in the substrate induce scattering in the graphene.

3. Experimental section

3.1. Graphene synthesis on various substrates

As shown in figure 1(a), 50 nm Ni thin film is prepared on high temperature compatible substrates (heavily doped Si with 300 nm SiO_2 , quartz, and sapphire) by sputtering (300 W). Graphene is deposited by a vertical cold wall CVD furnace (Black Magic, Aixtron). The samples are heated to 800°C at $200^\circ\text{C min}^{-1}$ rate and annealed for 5 min in H_2 atmosphere. Then, with 500 sccm Ar, 500 sccm H_2 and 10 sccm CH_4 , the temperature is elevated to 1000°C , and maintained for 5 min to grow graphene at 15 mbar. Finally, quench cooling ($300^\circ\text{C min}^{-1}$) is used to suppress the carbon segregation effect of Ni in order to attain a uniform number of layers. The whole procedure described above (including heating and cooling) is approximately 30 min.

3.2. Metal film etching

A PMMA resist layer is spun onto the as-grown graphene samples at 3000 r min^{-1} speed for 30 s. It is cured at 150°C

for 5 min. Then, the samples are immersed in a Ni etching solution ($\text{CuSO}_4\text{:HCl:H}_2\text{O} = 10\text{ g:50 ml:50 ml}$) for 10 min (figure S2). After the etching of Ni, the samples are kept in DI water for 15 min followed by blow dry with N_2 gas. The samples are post baked at $150\text{ }^\circ\text{C}$ for 10 min to remove the residue water and improve the graphene-substrate adhesion. Finally, the PMMA is removed by 15 min acetone bath and 5 min isopropanol rinse, ended with N_2 blow dry.

4. Conclusion

In conclusion, we have demonstrated a technical approach of growing lithography-free patterned CVD graphene directly on insulating substrates by etching sacrificial metal catalyst through a PMMA support layer. First, a thin layer of nickel film is evaporated onto the silicon dioxide substrate as the sacrificial catalyst. Then, graphene is grown by CVD on the upper surface of the Ni. In contrast to some previous reports, we have not found any noticeable graphene deposition beneath the Ni film through carbon segregation effect. After the growth, a PMMA polymer support layer is deposited on the graphene and the Ni is selectively removed by wet chemistry. The etchant directly penetrates the PMMA and makes the etching very efficient. The graphene lands on the insulating substrate naturally, adhered by van der Waals bonds. Compared to standard graphene transfer from a foreign substrate, here no mechanical manipulation is needed, and hence it leads to minimal damage in the graphene. The catalytic nature of the Ni is a fundamental advantage over other types of catalyst-free graphene growth. Also, since the shape of graphene is determined by the shape of Ni, which can be pre-patterned lithographically, the direct contact of graphene to photoresist can be avoided, making it possible to do lithography-free patterning in the graphene. Finally, we show the electrical measurements in the as-prepared graphene by fabricating and characterizing GFETs.

This is an attempt of simultaneously solving the currently existing bottlenecks in the graphene community, namely the transfer of graphene from metal catalysts to insulators, and the photoresist induced degradation during patterning. We note that these two problems are the major obstacles in the way of graphene's transition from academic labs to real applications. Although the demonstrated results need further incremental studies for refinement, the proof-of-principle experiments have already been accomplished. Therefore, we believe it is a step forward towards CVD graphene's commercial applications, where the process reliability and material quality are the most important factors. The proposed strategy is also generic because it can, in principle, be extended to grow other 2D materials with catalysts beyond nickel.

Acknowledgments

We acknowledge the support from National Key R&D Program of China (2018YFA0209000 and 2017YFB0403102),

National Natural Science Foundation of China (11674016), Beijing Natural Science Foundation (4172009), Beijing Municipal Commission of Science and Technology (Z161100002116032), Beijing Municipal Commission of Education (PXM2017_014204_500034), and Swedish Foundation for International Cooperation in Research and Higher Education (CH2015-6202).

ORCID iDs

Guanzhong Pan  <https://orcid.org/0000-0001-9973-866X>
Jie Sun  <https://orcid.org/0000-0002-6479-7771>

References

- [1] Geim A K and Novoselov K S 2007 *Nat. Mater.* **6** 183–91
- [2] Novoselov K S *et al* 2009 *Vacuum* **83** 1248–52
- [3] Novoselov K S *et al* 2004 *Science* **306** 666–9
- [4] Cote L J, Kim F and Huang J X 2009 *J. Am. Chem. Soc.* **131** 1043–9
- [5] Green A A and Hersam M C 2009 *Nano Lett.* **9** 4031–6
- [6] Gao W, Alemany L B, Ci L and Ajayan P M 2009 *Nat. Chem.* **1** 403–8
- [7] Berger C *et al* 2006 *Science* **312** 1191–6
- [8] Kedzierski J *et al* 2008 *IEEE Trans. Electron Devices* **55** 2078–85
- [9] Kim K S *et al* 2009 *Nature* **457** 706–10
- [10] Li X S *et al* 2009 *Science* **324** 1312–4
- [11] Zhan Z Y, Sun J, Liu L H, Wang E, Cao Y, Lindvall N, Skoblin G and Yurgens A 2015 *J. Mater. Chem. C* **3** 8634–41
- [12] Wang H P and Yu G 2016 *Adv. Mater.* **28** 4956–75
- [13] Sun J, Cole M T, Lindvall N, Teo K B K and Yurgens A 2012 *Appl. Phys. Lett.* **100** 022102
- [14] Bi H, Sun S R, Huang F Q, Xie X M and Jiang M H 2012 *J. Mater. Chem.* **22** 411–6
- [15] Kato T and Hatakeyama R 2012 *ACS Nano* **6** 8508–15
- [16] Wei D, Lu Y, Han C, Niu T, Chen W and Wee A T S 2013 *Angew. Chem., Int. Ed. Engl.* **52** 14121–6
- [17] Su C-Y *et al* 2011 *Nano Lett.* **11** 3612–6
- [18] Dong Y B *et al* 2018 *APL Mater.* **6** 026802
- [19] Peng Z, Yan Z, Sun Z and Tour J M 2011 *ACS Nano* **5** 8241–7
- [20] Yan Z, Peng Z, Sun Z, Yao J, Zhu Y, Liu Z, Ajayan P M and Tour J M 2011 *ACS Nano* **5** 8187–92
- [21] Sul O, Kim K, Choi E, Kil J, Park W and Lee S B 2016 *Nanotechnology* **27** 505205
- [22] Blake P *et al* 2007 *Appl. Phys. Lett.* **91** 063124
- [23] Reina A, Thiele S, Jia X, Bhaviripudi S, Dresselhaus M S, Schaefer J A and Kong J 2009 *Nano Res.* **2** 509–16
- [24] Ni Z, Wang Y, Yu T and Shen Z 2008 *Nano Res.* **1** 273–91
- [25] Geng D C *et al* 2012 *Proc. Natl Acad. Sci. USA* **109** 7992–6
- [26] Geng D C *et al* 2014 *Adv. Funct. Mater.* **24** 1664–70
- [27] Geng D C *et al* 2014 *Adv. Mater.* **26** 6423–9
- [28] Ishiyama C and Higo Y 2002 *J. Polym. Sci. Polym. Phys.* **40** 460–5
- [29] Hu S *et al* 2014 *Nature* **516** 227–30
- [30] Baraton L, He Z B, Lee C S, Maurice J L, Cojocaru C S, Gourgues-Lorenzon A F, Lee Y H and Pribat D 2011 *Nanotechnology* **22** 085601
- [31] Sun J, Lindvall N, Cole M, Teo K and Yurgens A 2011 *Appl. Phys. Lett.* **98** 252107